

The Impact of Print-and-Scan in Heterogeneous Morph Evaluation Scenarios

Richard E. Neddore
Clarkson University
Potsdam, NY, USA
neddore@clarkosn.edu

Zander W. Blasingame
Clarkson University
Potsdam, NY, USA
blasinzw@clarkson.edu

Chen Liu
Clarkson University
Potsdam, NY, USA
cliu@clarkson.edu

Abstract

Face morphing attacks present an emerging threat to the face recognition system. On top of that, printing and scanning the morphed images could obscure the artifacts generated during the morphing process, which makes morphed image detection even harder. In this work, we investigate the impact that printing and scanning has on morphing attacks through a series of heterogeneous tests. Our experiments show that we can increase the possibility of a false match by up to 5.64% for DiM and 16.00% for StyleGAN2 when providing an image that has been printed and scanned, regardless it is morphed or bona fide, to a Face Recognition (FR) system. Likewise, using Fréchet Inception Distance (FID) metric, strictly print-scanned morph attacks performed on average 9.185% stronger than non-print-scanned digital morphs.

1. Introduction

Face recognition (FR) systems have become one of the most widely used biometric modalities, ranging from security to identification applications in government offices, law enforcement, and visa management. These identification systems can prevent most unauthorized access while also maintaining low false rejection and acceptance rates, placing them among the best methods to reduce security vulnerabilities [1]. However, these systems still have susceptibilities, notably in the face of face morphing attacks. Face morphing attacks aim to exploit the intrinsic nature of FR classifiers that map biometric templates to a singular identity in a one-to-one map. To achieve this an attacker creates a morphed face incorporating the biometric traits and facial landmarks of two different identities and presenting a single image to an FR system. When the FR system is presented with a morphed image a vulnerability is created, forcing the FR system to register a match with two different identities violating the one-to-one mapping principle [2–6].

One area of notable concern is the use of morphed images in e-passports and machine-readable travel documents

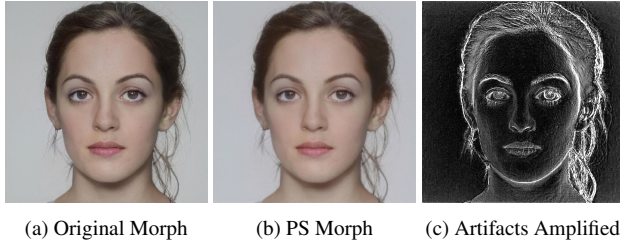
(MRTD) [7–9]. In cases where countries also utilize e-passports for not only renewal but also the issuance of documents this vulnerability is only amplified [10]. A person who is unauthorized or blacklisted may still be able to get access to restricted systems, areas, or travel if a morphed image is used in an e-passport or an MRTD.

The emergence of this threat has led to research and development of FR systems and Morphing Attack Detection (MAD) algorithms, which can be categorized into techniques that utilize feature extraction by deep learning models Single and Differential morph detection algorithms. MADs can be classified into two broad types of algorithms: Single-image MAD (S-MAD) and Differential MAD (D-MAD) [11]. While these systems have grown and D-MADs use a bona fide image to compare against a possible attack, the diversity in morphing techniques makes classification no easy feat. Attacks using generative models like Generative Adversarial Networks (GANs) [12] and landmark-based models that use biometric landmarks to make morphs [10] have developed and shown that FR systems still have difficulty detecting morphed images even with a bona fide for comparison. It should be noted that landmark-based attacks tend to contain more noticeable artifacts than representation-based attacks [10]. Recent works have shown that by taking an image and processing it using a method called printing and scanning, FR systems begin to struggle to classify whether the image is or is not a morphed image [13].

1.1. Contribution

Physical manipulation of these images can remove traces from the morphing algorithm and create a “new” image. This attack is particularly effective on FR systems that haven’t been trained to incorporate a printing and scanning style attack since the system cannot classify the unique artifacts generated during the printing and scanning process. When an image is printed, a unique type of artifact is introduced that masks and destroys the artifacts generated during the morphing process. Printing generates marks from where the ink was applied to the paper from rollers and

Figure 1. Artifacts on Morphed Image after Print and Scan



characteristics including, the absorption of the ink, the texture of the paper, and how the surface was handled both before and after printing, all cause the original image to be altered in small ways. Scanning also will leave traceable artifacts. The light from the scanner reflects off the page and can be seen in darker areas, like in the pupils, if done incorrectly. The scanner could also leave digital signatures if various post-processing effects were applied and saved to the image after undergoing scanning. The artifacts introduced during the print-scan process (as shown in Figure 1c) can be derived by subtracting the differences between the morphed image before (as shown in Figure 1a) and after being printed and scanned (as shown in Figure 1b).

This paper examines the implications that come from cross-testing a digitally altered image with one that has gone through stages of physical altering in the form of printing and scanning. The presentation of the attack being performed could introduce a type of bias associated with the presence of particular artifacts unique to each representation of media. This can be seen when introducing compression artifacts into images before evaluating their effectiveness against an FR system [14]. When comparing a digital morph to a print-scanned bona fide or a print-scanned morph to a digital bona fide, the mis-classification rate increases. The reference image should use the baseline modality for what particular artifacts are present in a morphed image.

The presence of inconsistent data when comparing potentially morphed images against bona fide images is an area lacking research. Performing a series of attacks with combinations of representation sources will provide a basis for a thorough examination of the impact that printed and scanned elements have on a biometric classification system. The evaluations will be performed in a heterogeneous testing environment set to highlight this vulnerability in FR systems' detection when one or more images, bona fide or morphed, have undergone printing and scanning.

2. Related works

While several groups are researching face morphing algorithms and FR detection, little work has been done to investigate and detect the threat of printed and scanned face

morphing attacks.

2.1. Print and Scan Simulation

Matteo *et al.* [15] focuses on addressing the possibility of security threats posed by printed and scanned face morphing in electronic identity documents. It highlights the challenges of detecting morphed images in cross-database testing and when dealing with printed and scanned images. The study introduces novel approaches to train Deep Neural Networks for morphing detection, including generating simulated printed-scanned images, data augmentation strategies, and pretraining on large face recognition datasets. The shortcoming of this study is that the printed and scanned morph images were simulated for their evaluation purposes, limiting the value of training with the generated data.

2.2. Printing and Scanning

Ngan *et al.* [13] addresses the need for datasets to train algorithms and FR systems for detection is a high-importance project. In that work under 7,000 images have undergone printing and scanning. The analysis, performed using a subset of visa-like images, underscores a critical concern: algorithms vary widely in their ability to discern between legitimate and morphed images once they have undergone the print-and-scan cycle. Algorithms showing low morph miss rates but very high false detection rates indicate these algorithms might classify most scanned photos as morphs even when they are not. Conversely, some single-image morph detectors exhibit low false detection rates but high morph miss rates, suggesting the potential reduction or elimination of morphing artifacts during the print-and-scan process.

Raja *et al.* [16] highlights the significance of the print-scan process as it reflects a real-world scenario in issuing identity documents. Printing and scanning a morphed image replicates the procedure often seen in getting a passport photo or identity card photo taken. Due to the nature of printing and scanning, the process can degrade image quality by introducing artifacts, changes in image resolution, and alterations in color and contrast which cause changes in the way FR systems perceive and quantify data. These changes could potentially impact the effectiveness of MAD algorithms by obscuring the artifacts that a face image has been morphed.

Zhang *et al.* [12] proposes a novel approach for generating face morphs that are harder for FR systems to detect. MIPGAN (Morphing through Identity Prior driven GAN) is meant to minimize the introduction of artifacts and leverage a different loss function to increase quality. Zhang *et al.* [12] also performed a series of experiments for different conditions including digital, printed and scanned, and compressed images after re-digitization. This setup shows

how the print-scan cycle affects the success rate of morphing attacks and the performance of detection algorithms in different scenarios. The study shows MIPGAN morphs maintain their attack effectiveness post-print-scan process, which points to the need for advanced MAD techniques that can effectively detect morphing attacks within scanned documents.

Raghavendra *et al.* [1] investigated both digital and print-scanned face morphs using fully connected layers of two CNNs. These morphed images were printed and scanned with various printers and scanners to vary the scope of their post-processing methods. Their results showed improved detection performance, emphasizing the method’s effectiveness. In cross-database evaluations, the ability to detect different sources and types of morphed face images, including those generated by different scanners. When different types of printers and scanners were used, differing artifacts became easier or harder to detect leading to some of their tests performing better than others.

3. Heterogeneous Morph Evaluation Scenarios

In this work “heterogeneous” encapsulates the varied nature of performing a set of evaluation scenarios using bona fides and morphed images that have and have not gone through a printing and scanning process. To compare the effectiveness of the print and scanned morphed image attack, in this work, the digital and the print-scanned images are tested against each other using different FR systems in a series of attack configurations: print-scan, PSD, DPS, and digital, as shown in Table 1. The difference in the attack configurations stems from whether the bona fide or the morphed images went through the print-scan process.

Table 1. Attack Configurations

Configuration	Morph	Bona Fide
Print-scan	Print-Scanned	Print-Scanned
PSD	Print-Scanned	Digital
DPS	Digital	Print-Scanned
Digital	Digital	Digital

Scenario 1: Print-scan vs Print-scan The print-scan style attack represents an attacker submitting a morphed photo that has been print-scanned and is submitted for use. This image is then compared to a bona fide image that has been printed and scanned into a database and is one of the identities in the morph.

Scenario 2: Print-scan vs Digital (PSD) The PSD-style attack represents an attacker submitting a morphed photo that has been print-scanned and is submitted for use. This image is then compared to a bona fide image that has not undergone any form of physical or digital manipulation.

Scenario 3: Digital vs Print-scan (DPS) The DPS-style attack represents an attacker submitting a morphed photo

that has not been print-scanned and is submitted for use. This image is then compared to a bona fide image that has been printed and scanned into a database.

Scenario 4: Digital vs Digital The digital-style attack represents an attacker submitting a morphed photo that has not been print-scanned and is submitted for use. This image is then compared to a bona fide image that has not undergone any form of physical or digital manipulation.

3.1. Relevance

With these configurations, the different artifacts from each presentation can be cross-tested to view the impact on FR systems’ ability to detect a morphed image under different circumstances. The PSD and DPS attack configurations are especially significant in testing the effectiveness of an FR system. These simulate the most likely scenario of what an attack would look like if performed outside the experiment environment. When submitting a photo for government identification, it will be compared to photos that are on file: either digital or a photo that has been print-scanned. In such cases, it is important to evaluate how a morphed image compares to images that come from different mediums.

4. Print-Scan Methodology

All print-scanned images are set at a 600×600 resolution with a pixel-per-inch value of 300 to replicate a passport photo. Photos are saved as a Portable Network Graphics (PNG) file to retain high-quality images. Doing so will prevent the file from introducing compression artifacts during post-processing, which could impact FR performance and detection. Printed images can develop flaws when International Color Consortium (ICC) profiles are improperly managed [17]. The implications of improper ICC profile management and compression artifacts can be observed in Figure 2.

ICC profiles manage the image’s exposure, saturation, and hue during the printing process and irregularities will occur when the incorrect profile is used. Photo printing paper has a linked ICC profile that must be selected before printing so the printing software can adjust settings accordingly. Photo printing paper also must be stored and handled with special care. Cotton gloves were always worn, and photo printing paper was stored in the plastic sleeve until printing was ready. These precautions were vital in keeping the photo paper from developing a warped surface or getting body oil on the print surface. The scan bed was also wiped with a microfiber cloth to remove dust and other particulates that settled on the surface between scans to avoid adding flaws to the image.

4.1. Equipment and Settings

A Canon Pixma Pro 100 Printer and Epson 850v Pro Scanner were used to print and scan all images evaluated

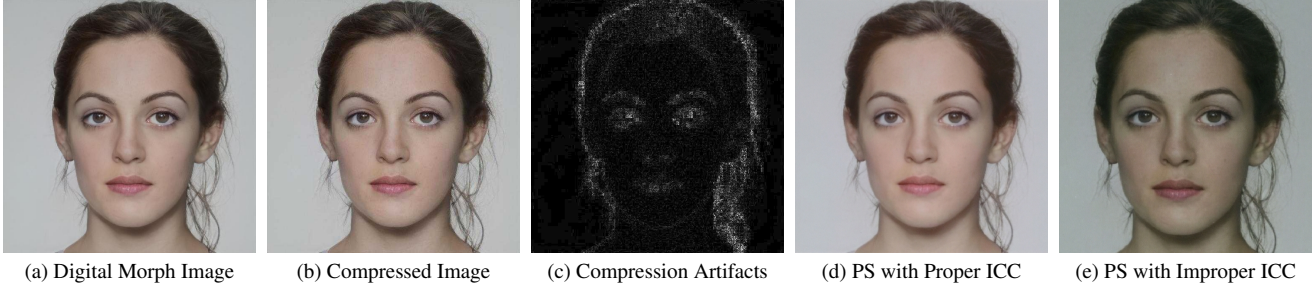


Figure 2. Importance of Quality Assurance

in this paper. Printing was handled using JavaScript and Extend-Script debugging scripts to interface with Adobe Photoshop for ICC Color Profile management to ensure proper image quality retention. High-quality and color-accurate printing is vital for testing and training. Improper ICC and print quality management will increase artifacts and result in poor image quality.

Default scanner software settings include presets and tools to improve image quality by increasing contrast or an image mask to the scanned image before saving occurs. The image quality improvements are fundamentally the same as altering an image in Photoshop, so image enhancement settings must be turned off before saving the image to avoid unintentionally reintroducing artifacts into the scanned images. Before scanning can occur, a sheet of images must be placed on the clean scanner bed and used to calibrate the scanner using the preview feature. Doing so allows settings to be adjusted and verified before scanning a printed dataset.

5. Experimental Setup

To evaluate the effectiveness of printing and scanning, morphing attacks were performed using four datasets against 6 different FR systems. All computation and evaluation was performed on two systems: One has dual Intel Xenon Silver 4114 CPUs and an NVIDIA Tesla V100 32GB GPU with CUDA version 10.1 and CUDNN version 8.4. The other system uses a Ryzen 9 5900x CPU and an NVIDIA Geforce RTX 3090TI 24GB GPU with CUDA version 11.3 and CUDNN version 8.4. The proposed morphing attacks, MAD algorithms, and FR systems were implemented in PyTorch. The print management and Photoshop scripts were implemented using extendscript. Other post-processing or landmark visualization scripts were implemented using Python.

5.1. Face Recognition Systems

Three well-known face recognition systems are utilized to evaluate the strength of printed and scanned morphing attacks: ElasticFace [18], Adaface [19], and ArcFace [20]. These FR systems determine a match by comparing feature vectors and finding images with various features

Table 2. Dataset Breakdown Investigated

Dataset	MA	Morphs	Bona fides
FRLL	StyleGAN2	1,222	204
	DiM	1,222	
FERET	StyleGAN2	529	1411
	DiM	529	
FRGC	StyleGAN2	964	3,038
	DiM	964	
Total		5,430	4,653

within a user-defined tolerance. The ArcFace was trained on the Glint360K dataset, which consists of 17,091,657 images from 360,232 individuals [21]. The ElasticFace and Adaface models are trained on the MS1M-ArcFace dataset. All three FR systems use different pre-processing pipelines to present the image as a passport photo. ArcFace, ElasticFace, and Adaface models use resized images. The image is cropped to a resolution of 112×112 and then normalized to have values in $[-1, 1]$.

5.2. Datasets

In this study, the FRGC v2.0 [22], FRLL [23], and FERET [24] datasets were used to determine the effectiveness of printed and scanned face morphing attacks. These datasets were chosen because they are used in NIST face morphing reports [13] and other face morphing analysis papers [11, 16]. Sarkar *et al.* [25] created the StyleGAN2 morphs for the FRGC, FRLL, and FERET datasets. We implemented the DiM algorithm from [10] to create DiM morphs for the FRGC, FRLL, and FERET datasets. For evaluation, the morphs, component identity pairs, and alternate bona fide identity images were printed and scanned. This process resulted in a total of 5,430 morphs and 4,653 bona fide images being printed and scanned, as shown in Table 2. The bona fide images for each dataset are shared between morphing attacks.

5.3. Morphing Attacks

This study investigates two different generative AI-based morphing attacks. The first method uses a GAN-based ar-

chitecture for its generative pipeline, while the second uses the Diffusion architecture to generate morphed images.

5.3.1 StyleGAN2

Sarkar *et al.* [3] introduces a method for creating face morphs using the StyleGAN2 architecture [25]. Generative Adversarial Networks (GANs) are a state-of-the-art single-step image generation model that aims to learn the data distribution by training in an adversarial manner. The generator network learns a mapping from the latent space to image space, allowing samples to be drawn from this latent space to sample the data space. For face morphing attacks an encoding strategy is deployed so that for a given image the latent code that represents it is found. The bona fide images used in the creation of the morphing attack are encoded into their latent representations. The latents are then morphed by averaging the latent vectors, resulting in the morphed latent. This morphed latent is then fed to the generator network constructing the morphed face.

5.3.2 DiM

Blasingame *et al.* [10] propose Diffusion Morphs (DiM) which use another kind of state-of-the-art generative model known as diffusion models. Diffusion models outperform GAN models on image synthesis; however, this comes at the cost of greater computational complexity during inference [26]. A diffusion process is described by a Stochastic Differential Equation (SDE) which slowly adds white noise to the original image, eventually degrading into pure white noise. Diffusion models learn how to reverse this SDE, enabling the sampling of images by starting with white noise and iteratively removing the noise over many steps until the denoised image is left. DiM uses a Diffusion Autoencoder [27] which is also conditioned on additional latent representation of the original image and provides an encoding strategy for mapping the original image into noise. Both the latent conditional and noise for the morphed images combined to create the morphed representation. The morphed conditional is constructed by averaging the conditionals of the two bona fide images. Conversely, the encoded noise of both images is blended using spherical interpolation with a factor of 0.5 [10]. The Diffusion Autoencoder then uses the morphed conditional and noise to create the morphed image.

5.4. Metrics

Several metrics are employed to evaluate the impact of printing and scanning on morphing attacks. These metrics were chosen due to their widespread use in face-morphing research.

5.4.1 MMPMR

The Mated Morph Presentation Match Rate (MMPMR) proposed by Scherhag *et al.* [28] is a widely used metric in evaluating the performance of a morphing attack [13, 29]. The MMPMR is defined as

$$M(\delta) = \frac{1}{M} \sum_{m=1}^M \left\{ \left[\min_{n \in \{1, \dots, N_m\}} S_m^n \right] > \delta \right\} \quad (1)$$

where δ is the verification threshold, S_m^n is the similarity score of the n -th subject of morph m , M is the total number of morphed images, and N_m is the total number of subjects contributing to morph m (often $N_m = 2$).

In the scenario in which multiple samples of a single subject are compared to a single morphed image, Scherhag *et al.* [28] recommend using the ProdAvg-MMPMR given as

$$M(\delta) = \frac{1}{M} \sum_{m=1}^M \left[\prod_{n=1}^{N_m} \left(\frac{1}{I_m^n} \sum_{i=1}^{I_m^n} \{S_m^{n,i} > \delta\} \right) \right] \quad (2)$$

where I_m^n is number of samples of subject n compared to morph m . As our evaluation compares multiple samples of the original subjects to a single morphed image, we use the ProdAvg-MMPMR, hereafter referred to as the MMPMR.

5.4.2 Classification Errors

Another widely used biometric metric is the ‘‘Attack Presentation Classification Error Rate’’ at a ‘‘Biometric Presentation Classification Error Rate’’, also referred to as APCER at BPCER. This metric quantifies the accuracy of the classifications using the rate at which fraudulent biometric samples are incorrectly classified as genuine and the rate at which genuine biometric samples are incorrectly classified as fraudulent. Using these two rates, a clear distinction in the performance of an FR system can be expressed.

The BPCER values chosen are thresholds at 0.1%, 1%, and 5%, respectively. A lower BPCER indicates a more strict classification system whereas a high APCER is a sign of a secure system with few false accepts. It is important to view the trade-offs across a range of rates as a system that cannot identify bona fide images properly isn’t useful for security. An optimal threshold for this is often determined when considering security requirements and risk assessments but can be viewed as a way to evaluate the robustness of an FR system.

The Equal Error Rate or EER represents the point at which the rate of false acceptances equals the rate of false rejections. This is the threshold at which an unauthorized user is just as likely to get into a system as they are rejected. This number helps classify the overall accuracy and reliability of a biometric system. A lower EER signifies a system

Table 3. MMPMR for all scenarios with FMR = 0.1%. Higher is better.

Morph	Scenario	FRL			FRGC			FERET		
		ArcFace	ElasticFace	AdaFace	ArcFace	ElasticFace	AdaFace	ArcFace	ElasticFace	AdaFace
DiM	Print-scan	93.13	84.78	89.20	47.98	37.10	44.42	69.54	61.35	63.65
DiM	PSD	92.39	85.11	89.69	48.47	39.45	42.55	67.10	62.75	66.51
DiM	DPS	93.37	84.62	89.36	52.16	40.03	42.40	69.58	62.41	67.83
DiM	Digital	92.96	85.19	90.18	52.44	41.08	42.05	70.43	62.75	66.37
StyleGAN2	Print-scan	5.89	3.76	5.16	0.88	1.01	1.45	0	0	0
StyleGAN2	PSD	5.32	3.27	6.46	0.89	1.07	1.13	0	0	0
StyleGAN2	DPS	6.14	3.36	5.24	1.48	1.36	1.36	0.78	0.41	1.23
StyleGAN2	Digital	5.89	3.27	6.55	1.38	1.21	1.25	1.01	0.63	0.82

adapted to rejecting unauthorized users while accepting authorized individuals.

The APCER at BPCER can be modeled graphically by plotting the false positive rate (FPR) on the x-axis and the false negative rate (FNR) on the y-axis. Doing so provides an in-depth representation of performance across a series of thresholds for the evaluated morphing attack scenarios for each dataset.

5.4.3 Fréchet Inception Distance (FID)

The visual fidelity of the DiM morphs is compared against the StyleGAN2 morphs across all morph evaluation scenarios. It is important to note that the ability to fool an FR system is not the same as having high visual fidelity. To evaluate the visual fidelity of the morphed images the Fréchet Inception Distance (FID) is used for the correlation to human assessment of fidelity [10,30]. The Fréchet distance is given as

$$\text{FID} = \|\mu_1 - \mu_2\|^2 + \text{Tr}(\sigma_1 + \sigma_2 - 2\sqrt{\sigma_1\sigma_2}) \quad (3)$$

where μ_1 is the mean of train data, σ_1 is the covariance of the train data, μ_2 is the mean of the test data σ_2 and is the covariance of the test data. In this work, the training data is the bona fide image and the testing data is the morphed image. The metric is defined as the Fréchet distance between two Gaussian distributions each representing the activations of the deepest layer of an Inception v3 network induced by images from the generated and target distributions [31].

While the use of FID has received negative feedback in terms of value and usefulness in determining the visual fidelity of a morph, the use case when comparing data across different post-processing modalities becomes clear. Since the metric compares the pixel average across Gaussian distributions, a difference in how digital morphs and printed and scanned morphs are observed becomes more apparent. The differing use case allows for this work to show how printed and scanned elements leverage the physical characteristics introduced and discussed in Section 1.1.

6. Results

To evaluate the effectiveness of each attack, various metrics were used highlighting vulnerabilities in the examined FR systems and the strength of different morphing attacks. The DiM and StyleGAN2 morphs are then evaluated against ArcFace, ElasticFace, and AdaFace. This series of attacks is then repeated for the FRL, FERET, and FRGC datasets across the different evaluation scenarios seen in Table 1.

6.1. Vulnerability Study

Table 3 presents the MMPMR results for FRL, FRGC, and FERET, respectively. The MMPMR was evaluated at a false match rate (FMR) at 0.1% for all evaluated morphing attacks, for each dataset, and for each evaluation scenario. It should be noted that DiM morphs perform better than their GAN-based counterparts despite their high visual fidelity. This is consistent with prior work and the state of the effectiveness of GAN-based morphing attacks *et al.* [3].

In terms of the MMPMR for FRL, it is observed to have the highest metrics overall across both the DiM and StyleGAN2 morphs. This phenomenon is likely due to the lack of a diverse collection of bona fide subjects used in the comparison metric. The dataset only has two bona fide images associated with each identity in contrast to FRGC and FERET which have a larger collection of associated bona fide images. MMPMR metrics are highly influenced by the number of bona fide comparisons that can be made as every failed attempt at verification decreases the attack score.

In terms of the MMPMR for FERET, it is observed to have the lowest MMPMR of the StyleGAN2 print-scan morphs evaluated. This phenomenon is likely due to the inherited characteristics of the morphs from the FERET dataset and the weakness of StyleGAN2 morphs discussed above. The bona fide images from this dataset have particularly low contrast, issues with sharpness, and uneven lighting. The DiM algorithm handled these inconsistencies well and produced better morphs with clearer characteristics, which made the printing and scanning process more effective.

In terms of the MMPMR for FRGC, it is observed to

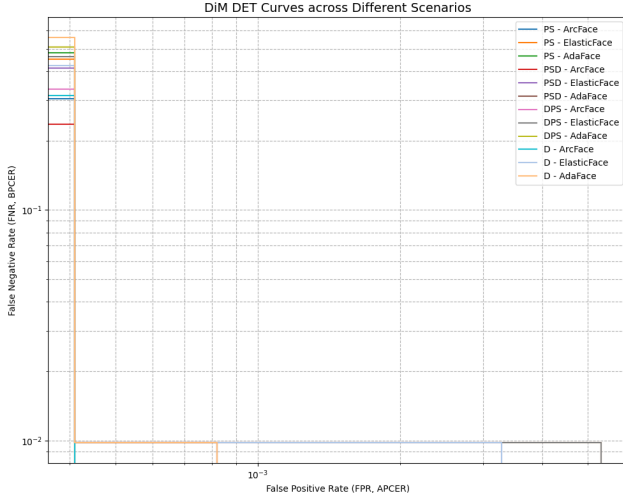


Figure 3. FRLI DET DiM

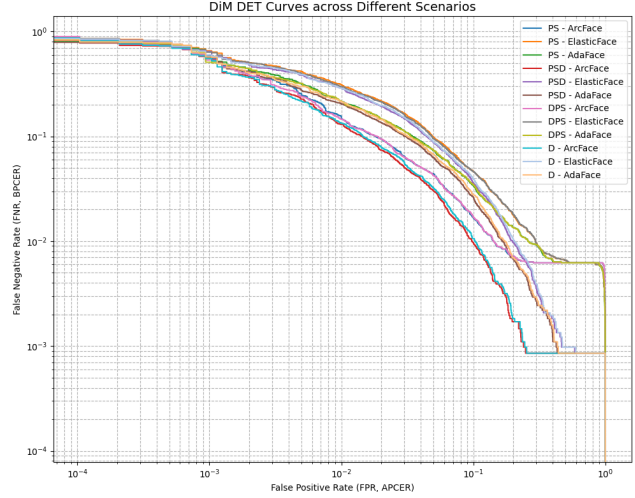


Figure 5. FRGC DET DiM

have the lowest DiM MMPMR overall, however, that does not mean that the morphs performed poorly. The FRGC dataset had the most bona fide images per each identity overall which similarly to the data from FRLI skews the overall evaluation. FRGC had the least variance of all the evaluated data indicating similarities between the digital and print-scanned bona fides.

The evaluations performed on attack scenarios containing print-scanned elements performed up to 5.64% better for DiM morphs and up to 16.0% better for the StyleGAN2 morphs. Not every evaluation favors attack scenarios containing print-scanned images. This is observed in the DiM evaluations that biased the strictly digital evaluation but were within 2.63% of the attacks with print-scanned properties. The StyleGAN2 morphs have a greater variance due to the poor-quality morphs.

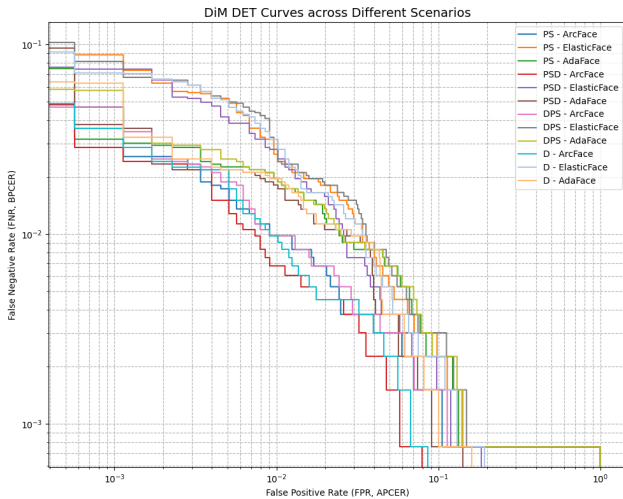


Figure 4. FERET DET DiM

Across the FRLI, FERET, and FRGC datasets, the morphing attack evaluations exhibit a pattern favoring attack scenarios containing print-scanned elements. Due to the lack of bona fide representations in the FRLI dataset, DET Curves are abnormal, as seen in Figure 3, the plot for the FRLI DiM morphs contains a limited number of points, one for each bona fide image. The curves that start with high FNRs even at low FPRs show an immediate weakness in the FR detection algorithm, suggesting that an attacker could potentially go undetected more easily with these systems. The scenarios that contain a printed and scanned element performed better or the same as the strictly digital scenarios, however, without additional bona fide data, it is hard to make a more exact conclusion.

The close grouping of the graphs in Figure 4 indicates that there is a degree of variability across the scenarios evaluated, which is to be expected. The mixed morph evaluations and print-scan scenarios exhibit higher APCER values across the graphs. These scenarios show a significant degree of vulnerability across all evaluated FR systems, meaning that it is hard to properly classify attacks from these scenarios as morphs or bona fides. The data from FRGC shown in Figure 5 follows an even closer grouping of data in the low APCER and high BPCER region. Towards the high APCER region, there is an increase in the degree of variability across the scenarios evaluated, which helps illustrate areas of weakness for the dataset. The print-scan scenarios exhibit higher APCER values across the graphs, showing a significant degree of vulnerability across all evaluated FR systems. The degree of effectiveness is not as high as seen in FERET, although that does not make the data any less meaningful. Like FERET, the scenarios examined illustrate that it is hard to properly classify attacks containing printed and scanned morphs or bona fides. In particular, ArcFace has the hardest time classifying an image in a fully print-

scanned attack across all three datasets, with fully digital attacks in a close second in terms of strength. ArcFace has less error when given heterogeneous data, but still shows vulnerability towards printed and scanned morphs over digital morphs during attacks. AdaFace struggles to classify all attacks equally from the FERET dataset but shows minimal variation in attacks from FRLL and FRGC with low false negative rates overall. Slight deviations in variance are shown across all three datasets, however, indicating that overall performance is consistent. This is a strength against weaker morphs from a particular dataset but becomes a weakness when a morphing technique becomes better and more advanced. Lastly, ElasticFace shows signs of being the most secure system out of the evaluated FR systems. Across all three datasets, ElasticFace maintains the lowest false positive rates with a low number of false negatives. The performance of the system tends to trend towards detecting all attacks similarly showing little vulnerability to heterogeneous morphing attacks, unlike the other evaluated systems.

6.2. Visual Fidelity Analysis

Table 4 shows the FID metrics across all heterogeneous morph evaluation scenarios. Overall the strictly print-scanned scenario shows a 9.185% increase in visual fidelity over the strictly digital scenario. This is indicative of printing and scanning masking morphing artifacts, as seen in Figure 1. The inherited differences between printed and scanned vs digital images impact the comparison for FID and as a result, perform better than strictly digital morphs in terms of visual fidelity. The heterogeneous morph evaluation between digital and print-scanned data scores worse on average than homogeneous morph evaluation scenarios. This likely stems from the appearance of artifacts that are unique to each method of presentation leading to a homogeneous bias. FRLL had the highest FID biasing in the strictly digital comparison over comparisons with printed and scanned elements for DiM morphs. FERET likewise had the highest StyleGAN2 FID scores with a similar bias. The remaining morphs all performed better in scenarios involving a print-scanned element indicating higher fidelity among print-scanned images.

Table 4. FID. Lower is better.

Morph	Scenario	FRLL	FERET	FRGC
DiM	Print-scan	46.18	44.31	52.94
DiM	PSD	45.88	52.20	54.99
DiM	DPS	57.17	60.08	69.93
DiM	Digital (D)	42.98	57.40	61.82
StyleGAN2	Print-scan	36.55	29.21	61.05
StyleGAN2	PSD	45.88	39.19	72.30
StyleGAN2	DPS	57.17	30.43	59.08
StyleGAN2	Digital (D)	42.98	27.91	71.91

7. Conclusion

By introducing a printed and scanned element into a morph evaluation, the ability to discriminate between a morphed image and a bona fide image becomes more difficult. This heterogeneous evaluation scenario leverages the introduction of printing and scanning artifacts into morphed images since they can mask artifacts generated during morphing while also increasing the overall visual fidelity of morphs. The method of printing and scanning followed in this work produced high-quality morphs given that data was of high quality before printing. This process generated a total of 10,083 printed and scanned bona fide and morphed images. These morphs outperformed the strictly digital morph attack scenario in the presence of printing and scanning across a vulnerability study and an analysis of visual fidelity.

7.1. Reproducibility Statement

To ensure the reproducibility and completeness of this work an appendix is attached with two primary sections. Appendix A provides the implementation details and the repositories for referenced models and data pipelines. The equipment settings are also discussed in this section. In Appendix B we provide additional results that were unable to be included in the main section of this paper but still pertain to the scope of this work.

7.2. Limitations and Future Work

Despite the range of evaluations and scenarios examined to test the effectiveness of heterogeneous morph attacks, the scope of this work covers only two morphing algorithms across three datasets. Repeating the steps followed in this work with varied morphing methods would help support the findings made in Section 6. Performing experiments with more FR systems and with single-image morph attack detectors (S-MADs), using additional classifying metrics like Morphing Attack Potential [15] would provide additional information for allowing for better comparisons between data [32].

A second limitation would be the range of equipment used to generate the printed and scanned images. The evaluation performed reflects only a portion of the possible impacts associated with ICC profiles, ink types, printing, and scanning methods. The performance against FR systems may not fluctuate a great amount but there will still be differences that can be better observed and tested across a variety of printers and scanners. The same can be said for differing the types of printer paper that images are printed and scanned on. Texture, sheen, and paper quality play a significant role in the fidelity and characteristics removed or added to images after printing and scanning. The presence of introducing and removing artifacts embedded in latent color

space that are attached to biometric landmarks is one area in which varying equipment would allow for deeper examinations into the unseen changes of printing and scanning [33].

References

- [1] R. Raghavendra, K. B. Raja, S. Venkatesh, and C. Busch, "Transferable deep-cnn features for detecting digital and print-scanned morphed face images," in *IEEE Conf. on Computer Vision and Pattern Recognition Workshops (CVPRW)*, 2017, pp. 1822–1830. [1](#), [3](#)
- [2] Z. Blasingame and C. Liu, "Leveraging adversarial learning for the detection of morphing attacks," *2021 IEEE International Joint Conference on Biometrics (IJCB)*, pp. 1–8, 2021. [1](#)
- [3] E. Sarkar, P. Korshunov, L. Colbois, and S. Marcel, "Are gan-based morphs threatening face recognition?" in *ICASSP 2022 - 2022 IEEE International Conference on Acoustics, Speech and Signal Processing (ICASSP)*, 2022, pp. 2959–2963. [1](#), [5](#), [6](#)
- [4] L. Colbois and S. Marcel, "On the detection of morphing attacks generated by gans," in *2022 International Conference of the Biometrics Special Interest Group (BIOSIG)*, 2022, pp. 1–5. [1](#)
- [5] R. Raghavendra, K. B. Raja, and C. Busch, "Detecting morphed face images," in *IEEE 8th Int'l Conf. on Biometrics Theory, Applications and Systems (BTAS)*, 2016, pp. 1–7. [1](#)
- [6] M. Ferrara, A. Franco, and D. Maltoni, *On the Effects of Image Alterations on Face Recognition Accuracy*. Cham: Springer International Publishing, 2016, pp. 195–222. [Online]. Available: https://doi.org/10.1007/978-3-319-28501-6_9 [1](#)
- [7] U. Scherhag, C. Rathgeb, J. Merkle, R. Breithaupt, and C. Busch, "Face recognition systems under morphing attacks: A survey," *IEEE Access*, vol. 7, pp. 23 012–23 026, 2019. [1](#)
- [8] F. Peng, L.-B. Zhang, and M. Long, "Fd-gan: Face demorphing generative adversarial network for restoring accomplice's facial image," *IEEE Access*, vol. 7, pp. 75 122–75 131, 2019. [1](#)
- [9] M. Hamza, S. Tehsin, M. Humayun, M. F. Almufareh, and M. Alfayad, "A comprehensive review of face morph generation and detection of fraudulent identities," *Applied Sciences*, vol. 12, no. 24, 2022. [Online]. Available: <https://www.mdpi.com/2076-3417/12/24/12545> [1](#)
- [10] Z. W. Blasingame and C. Liu, "Leveraging diffusion for strong and high quality face morphing attacks," *IEEE Transactions on Biometrics, Behavior, and Identity Science*, vol. 6, no. 1, pp. 118–131, 2024. [1](#), [4](#), [5](#), [6](#)
- [11] H. Zhang, S. Venkatesh, R. Ramachandra, K. Raja, N. Damer, and C. Busch, "Mipgan – generating strong and high quality morphing attacks using identity prior driven gan," 2021. [1](#), [4](#)
- [12] —, "Mipgan—generating strong and high quality morphing attacks using identity prior driven gan," *IEEE Transactions on Biometrics, Behavior, and Identity Science*, vol. 3, no. 3, pp. 365–383, 2021. [1](#), [2](#)
- [13] M. Ngan, P. Grother, K. Hanaoka, and J. Kuo, "Face recognition vendor test (frvt) part 4: Morph - performance of automated face morph detection," 2020-03-06 2020. [1](#), [2](#), [4](#), [5](#)
- [14] U. Scherhag, C. Rathgeb, and C. Busch, *Face Morphing Attack Detection Methods*. Cham: Springer International Publishing, 2022, pp. 331–349. [Online]. Available: https://doi.org/10.1007/978-3-030-87664-7_15 [2](#)
- [15] M. Ferrara, A. Franco, and D. Maltoni, "Face morphing detection in the presence of printing/scanning and heterogeneous image sources," *IET Biometrics*, Feb 2021. [Online]. Available: <http://dx.doi.org/10.1049/bme2.12021> [2](#), [8](#)
- [16] K. Raja et al., "Morphing attack detection - database, evaluation platform and benchmarking," *IEEE Transactions on Information Forensics and Security*, pp. 1–1, 2020. [2](#), [4](#)
- [17] International Color Consortium, *ICC Specification ICC.1:2004-10 (Profile version 4.3.0.0)*, December 2010, available online at <https://www.color.org/specification/icc1v43.2010-12.pdf>. [3](#)
- [18] F. Boutros, N. Damer, F. Kirchbuchner, and A. Kuijper, "Elasticface: Elastic margin loss for deep face recognition," in *Proceedings of the IEEE/CVF Conference on Computer Vision and Pattern Recognition (CVPR) Workshops*, June 2022, pp. 1578–1587. [4](#)
- [19] M. Kim, A. K. Jain, and X. Liu, "Adaface: Quality adaptive margin for face recognition," in *Proceedings of the IEEE/CVF Conference on Computer Vision and Pattern Recognition*, 2022. [4](#)
- [20] J. Deng, J. Guo, N. Xue, and S. Zafeiriou, "Arcface: Additive angular margin loss for deep face recognition," in *Proceedings of the IEEE Conference on Computer Vision and Pattern Recognition*, 2019, pp. 4690–4699. [4](#)
- [21] X. An, X. Zhu, Y. Gao, Y. Xiao, Y. Zhao, Z. Feng, L. Wu, B. Qin, M. Zhang, D. Zhang, and Y. Fu, "Partial fc: Training 10 million identities on a single machine," in *2021 IEEE/CVF International Conference on Computer Vision Workshops (ICCVW)*, 2021, pp. 1445–1449. [4](#)
- [22] P. Phillips, P. Flynn, T. Scruggs, K. Bowyer, J. Chang, K. Hoffman, J. Marques, J. Min, and W. Worek, "Overview of the face recognition grand challenge," in *2005 IEEE Computer Society Conference on Computer Vision and Pattern Recognition (CVPR'05)*, vol. 1, 2005, pp. 947–954 vol. 1. [4](#)
- [23] L. DeBruine and B. Jones, "Face Research Lab London Set," 5 2017. [Online]. Available: https://figshare.com/articles/dataset/Face_Research_Lab_London_Set/5047666 [4](#)
- [24] P. Phillips, H. Wechsler, J. Huang, and P. J. Rauss, "The feret database and evaluation procedure for face-recognition algorithms," *Image Vis. Comput.*, vol. 16, pp. 295–306, 1998. [4](#)

- [25] T. Karras, S. Laine, M. Aittala, J. Hellsten, J. Lehtinen, and T. Aila, “Analyzing and improving the image quality of stylegan,” in *2020 IEEE/CVF Conference on Computer Vision and Pattern Recognition (CVPR)*, 2020, pp. 8107–8116. 4, 5
- [26] P. Dhariwal and A. Nichol, “Diffusion models beat gans on image synthesis,” in *Advances in Neural Information Processing Systems*, M. Ranzato, A. Beygelzimer, Y. Dauphin, P. Liang, and J. W. Vaughan, Eds., vol. 34. Curran Associates, Inc., 2021, pp. 8780–8794. [Online]. Available: <https://proceedings.neurips.cc/paper/2021/file/49ad23d1ec9fa4bd8d77d02681df5cfa-Paper.pdf> 5
- [27] K. Preechakul, N. Chatthee, S. Wizadwongsa, and S. Suwanakorn, “Diffusion autoencoders: Toward a meaningful and decodable representation,” in *Proceedings of the IEEE/CVF Conference on Computer Vision and Pattern Recognition (CVPR)*, June 2022, pp. 10 619–10 629. 5
- [28] U. Scherhag, A. Nautsch, C. Rathgeb, M. Gomez-Barrero, R. N. J. Veldhuis, L. Spreeuwers, M. Schils, D. Maltoni, P. Grother, S. Marcel, R. Breithaupt, R. Ramachandra, and C. Busch, “Biometric systems under morphing attacks: Assessment of morphing techniques and vulnerability reporting,” in *2017 International Conference of the Biometrics Special Interest Group (BIOSIG)*, 2017, pp. 1–7. 5
- [29] M. Ferrara, A. Franco, D. Maltoni, and C. Busch, “Morphing attack potential,” in *2022 International Workshop on Biometrics and Forensics (IWBF)*, 2022, pp. 1–6. 5
- [30] M. Lucic, K. Kurach, M. Michalski, O. Bousquet, and S. Gelly, “Are gans created equal? a large-scale study,” in *Proceedings of the 32nd International Conference on Neural Information Processing Systems*, ser. NIPS’18. Red Hook, NY, USA: Curran Associates Inc., 2018, p. 698–707. 6
- [31] M. Seitzer, “pytorch-fid: FID Score for PyTorch,” <https://github.com/mseitzer/pytorch-fid>, August 2020, version 0.2.1. 6
- [32] Z. W. Blasingame and C. Liu, “Fast-dim: Towards fast diffusion morphs,” 2024. 8
- [33] I. Batskos, L. Spreeuwers, and R. Veldhuis, “Visualizing landmark-based face morphing traces on digital images,” *Frontiers in Computer Science*, vol. 5, 2023. [Online]. Available: <https://www.frontiersin.org/articles/10.3389/fcomp.2023.981933/full> 9

A. Implementation Details

Before being printed and scanned the images to be printed are resized and saved as PNG's. Images are then digitally arranged on an $8.5inch \times 12inch$ blank PNG. Scripts are used to send the pages of images to Adobe Photoshop for print management to maintain ICC profiles. After printing and scanning, the images go through a series of post-processing scripts that isolate, crop, rename, and resize images to resemble the original digital image for testing, evaluation, and quality control purposes.

A.1. Repositories Used

For reproducibility purposes, we provide a list of links to the official repositories of other works used in this paper.

1. The ArcFace models, MS1M-RetinaFace dataset, and MS1M-ArcFace dataset can be found at <https://github.com/deepinsight/insightface>.
2. The ElasticFace model can be found at <https://github.com/fdbtrs/ElasticFace>.
3. The AdaFace model can be found at <https://github.com/mk-minchul/AdaFace>.
4. The VGGFace2 dataset and model can be found https://github.com/ox-vgg/vgg_face2.
5. The official Diffusion Autoencoders repository is found at <https://github.com/phizaz/diffae>.
6. The implementation of FID can be found at <https://pytorch.org/ignite/generated/ignite.metrics.FID.html>

B. Additional Results

While the StyleGAN2 DET curves for FRGC in Figure 8 and FERET in Figure 7 are not abnormal, the DET curve for the FRL dataset in Figure 6 is completely blank. This is also the case for the APCER @ BPCER in Table 5. This is likely the case because of the poor data that comes from the morphs being GAN-based and the limited availability of bona fides for comparison purposes.

The data from FERET and FRGC shown in Table 6 and Table 7, respectively, have a close grouping of data with low error rates and low false positive rates at lower BCPER values. The print-scan scenarios exhibit higher APCER values across both tables. Figure 7 and Figure 8 likewise show an area of vulnerability across all evaluated FR systems.

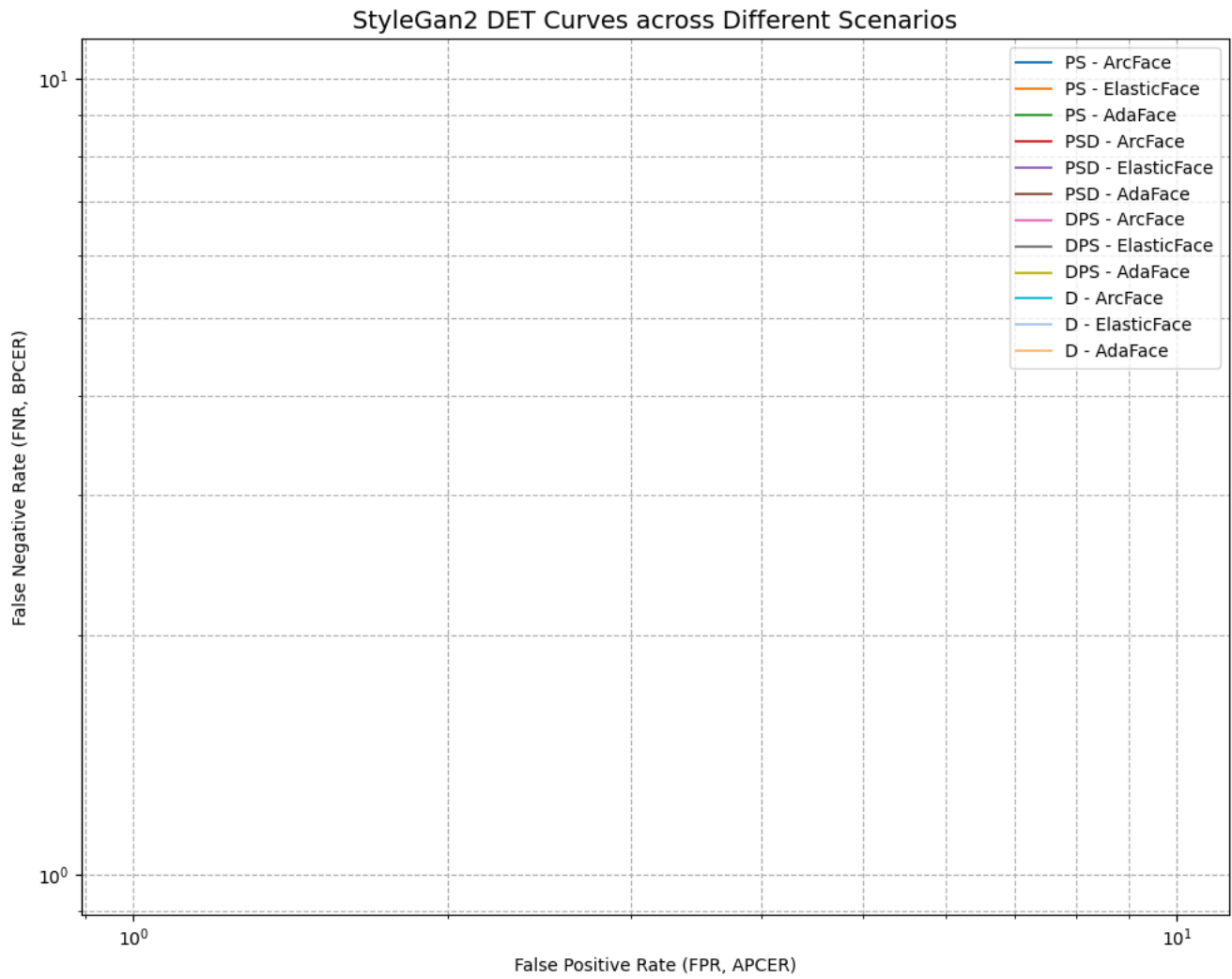


Figure 6. FRL DET StyleGAN2

StyleGan2 DET Curves across Different Scenarios

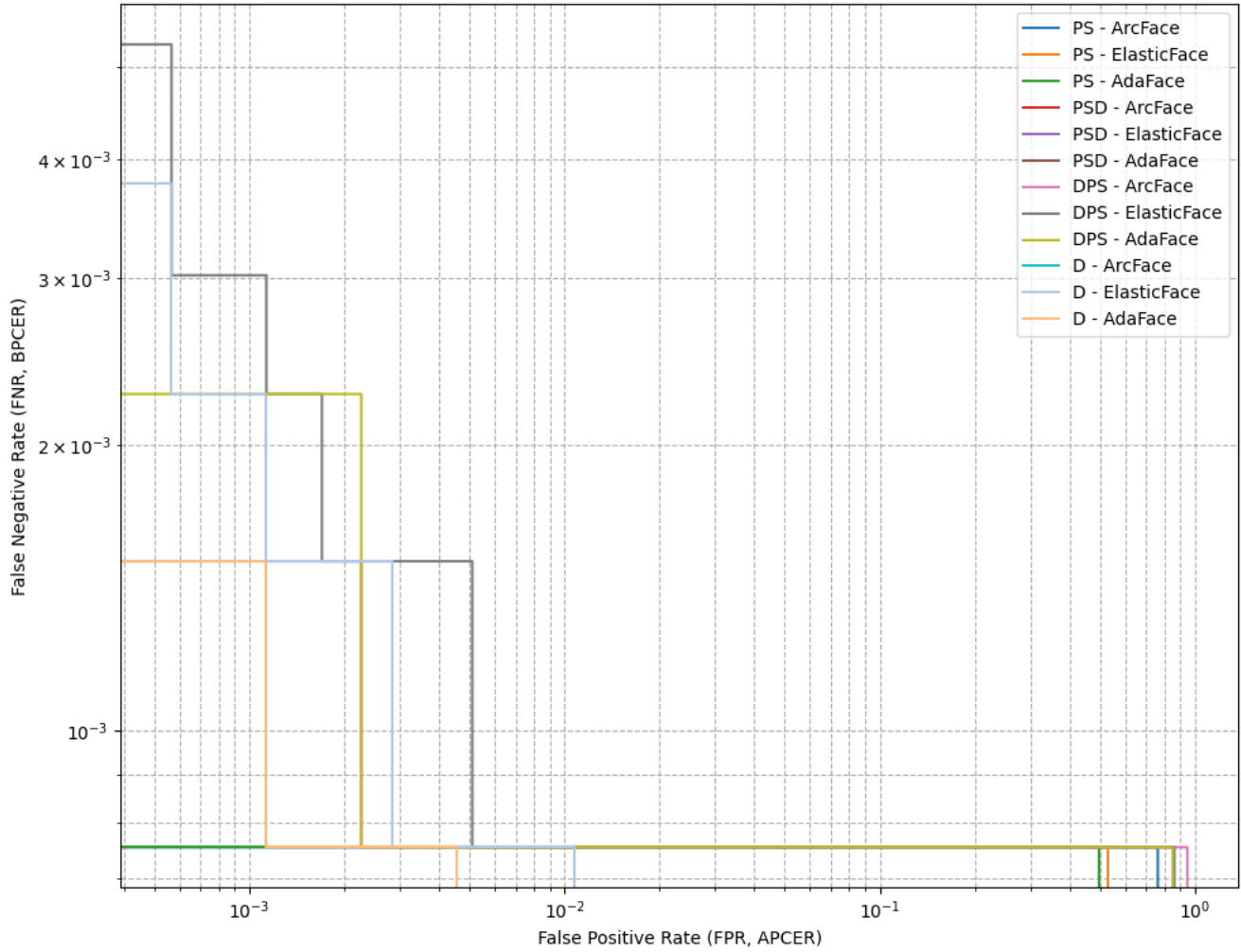


Figure 7. FERET DET StyleGAN2

StyleGan2 DET Curves across Different Scenarios

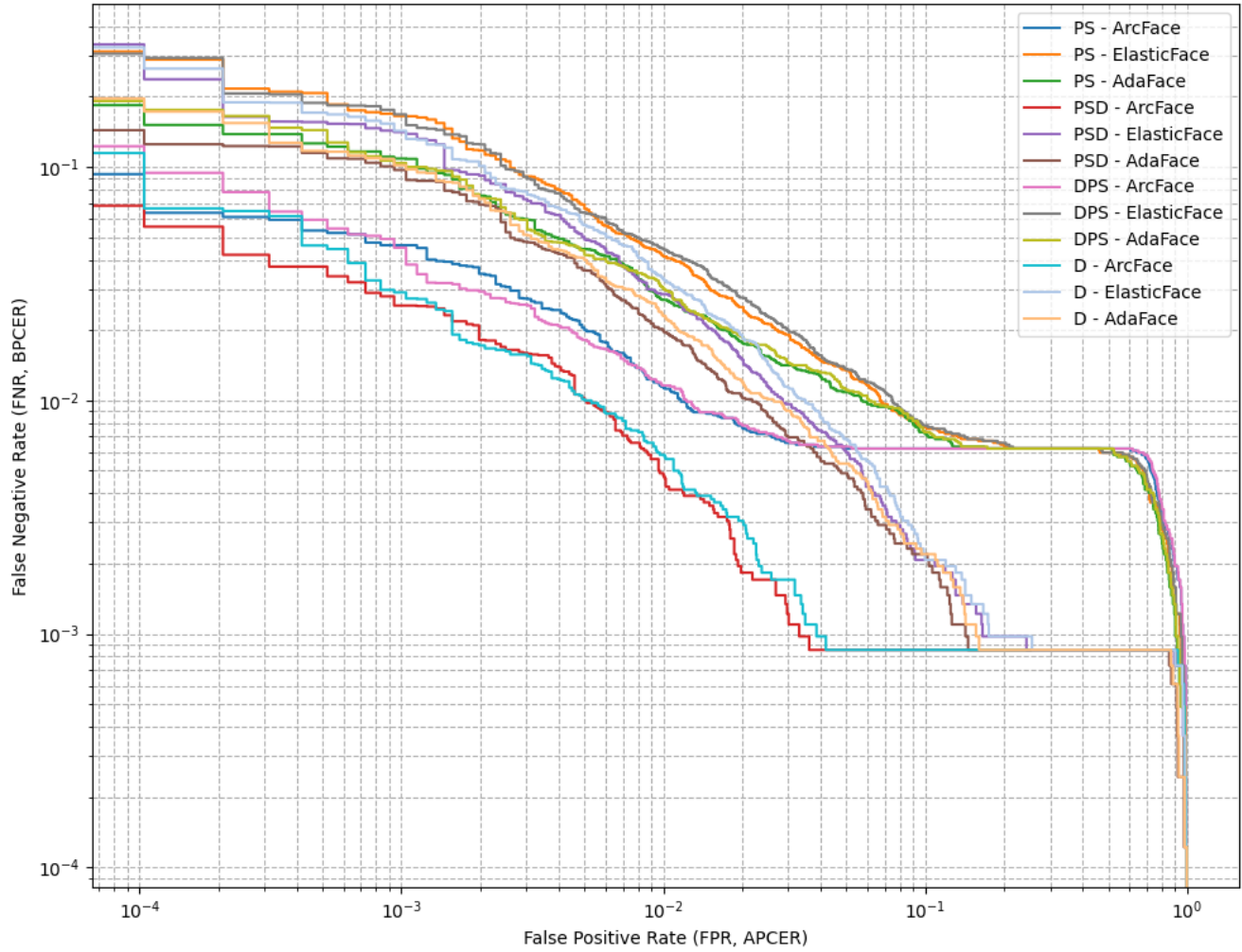


Figure 8. FRGC DET StyleGAN2

Table 5. FRLI APCER @ BPCER

Scenario	FR System	Morph	EER (%)	0.1%	1.0%	5.0%
DiM	Print-scanned	ArcFace	0.08	0.08	0.04	0.04
		ElasticFace	0.53	0.53	0.04	0.04
		AdaFace	0.04	0.04	0.04	0.04
	PSD	ArcFace	0.04	0.04	0.04	0.04
		ElasticFace	0.33	0.33	0.04	0.04
		AdaFace	0.08	0.08	0.04	0.04
	DPS	ArcFace	0.08	0.08	0.04	0.04
		ElasticFace	0.53	0.53	0.04	0.04
		AdaFace	0.04	0.04	0.04	0.04
	Digital	ArcFace	0.04	0.04	0.04	0.04
		ElasticFace	0.33	0.33	0.04	0.04
		AdaFace	0.08	0.08	0.04	0.04
StyleGAN2	Print-scanned	ArcFace	0	0	0	0
		ElasticFace	0	0	0	0
		AdaFace	0	0	0	0
	PSD	ArcFace	0	0	0	0
		ElasticFace	0	0	0	0
		AdaFace	0	0	0	0
	DPS	ArcFace	0	0	0	0
		ElasticFace	0	0	0	0
		AdaFace	0	0	0	0
	Digital	ArcFace	0	0	0	0
		ElasticFace	0	0	0	0
		AdaFace	0	0	0	0

Table 6. FERET APCER @ BPCER

Scenario	FR System	Morph	EER (%)	0.1%	1.0%	5.0%
DiM	Print-scanned	ArcFace	0.96	10.54	0.91	0
		ElasticFace	1.87	14.00	3.40	0.51
		AdaFace	1.53	13.32	2.44	0.06
	PSD	ArcFace	0.85	5.78	0.74	0
		ElasticFace	1.64	11.96	2.61	0.34
		AdaFace	1.42	9.07	2.72	0.06
	DPS	ArcFace	0.96	11.34	0.91	0
		ElasticFace	1.93	14.91	3.57	0.51
		AdaFace	1.53	14.17	2.49	0.11
	Digital	ArcFace	0.96	6.75	0.91	0
		ElasticFace	1.64	13.10	3.40	0.51
		AdaFace	1.47	10.03	2.89	0.11
StyleGAN2	Print-scanned	ArcFace	1.08	96.18	1.17	0.07
		ElasticFace	2.26	93.86	6.77	0.75
		AdaFace	1.88	90.16	5.77	0.39
	PSD	ArcFace	0	0	0	0
		ElasticFace	0	0	0	0
		AdaFace	0	0	0	0
	DPS	ArcFace	0.17	0.23	0	0
		ElasticFace	0.17	0.51	0	0
		AdaFace	0.23	0.23	0	0
	Digital	ArcFace	0	0	0	0
		ElasticFace	0.17	0.28	0	0
		AdaFace	0.11	0.11	0	0

Table 7. FRGC APCER @ BPCER

Scenario	FR System	Morph	EER (%)	0.1%	1.0%	5.0%
DiM	Print-scanned	ArcFace	4.63	99.92	14.24	4.11
		ElasticFace	6.95	99.84	29.55	9.19
		AdaFace	6.03	99.73	26.14	7.16
	PSD	ArcFace	3.96	23.99	9.85	3.02
		ElasticFace	6.54	46.57	19.82	8.12
		AdaFace	5.50	42.42	16.63	6.12
	DPS	ArcFace	4.59	99.93	14.24	4.12
		ElasticFace	6.87	99.86	29.61	9.27
		AdaFace	6.03	99.78	26.17	7.06
	Digital	ArcFace	4.12	24.53	10.37	3.23
		ElasticFace	6.63	47.29	20.55	8.29
		AdaFace	5.70	43.39	17.36	6.53
StyleGAN2	Print-scanned	ArcFace	1.08	96.18	1.17	0.07
		ElasticFace	2.26	93.86	6.77	0.75
		AdaFace	1.88	90.16	5.77	0.39
	PSD	ArcFace	0.71	3.30	0.51	0.02
		ElasticFace	1.77	16.55	2.85	0.50
		AdaFace	1.44	14.24	2.19	0.26
	DPS	ArcFace	1.13	96.41	1.23	0.08
		ElasticFace	2.37	94.62	7.50	0.79
		AdaFace	1.93	90.84	6.20	0.35
	Digital	ArcFace	0.75	3.84	0.53	0.04
		ElasticFace	1.95	17.48	3.48	0.63
		AdaFace	1.56	15.63	2.65	0.31